NASA TN D-257

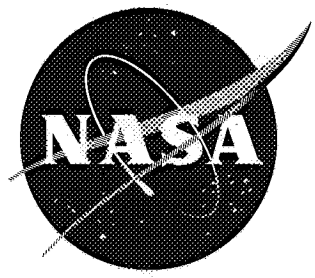

# TECHNICAL NOTE

## D-257

# PERFORMANCE INVESTIGATION OF A NONPUMPING ROCKET-EJECTOR SYSTEM FOR ALTITUDE SIMULATION

By Anthony Fortini

Lewis Research Center
Cleveland, Ohio

NATIONAL AERONAUTICS AND SPACE ADMINISTRATION
WASHINGTON

December 1959

NATIONAL AERONAUTICS AND SPACE ADMINISTRATION

TECHNICAL NOTE D-257

# PERFORMANCE INVESTIGATION OF A NONPUMPING ROCKET-EJECTOR SYSTEM FOR ALTITUDE SIMULATION

By Anthony Fortini



## SUMMARY

The effect of various dimensions on the performance of a prototype, nonpumping cylindrical-rocket-ejector system was studied both theoretically and experimentally. The rocket-ejector system contained a convergent-divergent nozzle with a nozzle exit-to-throat area ratio of 9. Various length and diameter ejector tubes enclosed the nozzle. High-pressure nitrogen gas flowed through the nozzle and served as the pumping fluid.

The cross-sectional area ratio of ejector tube to nozzle throat and the ratio of ejector-tube length to diameter were investigated. A range of ejector-tube area ratios from 16 to 49 and ejector-tube length-to-diameter ratios from 2.67 to 12.0 was studied for various ratios of pumping pressure to atmospheric pressure. The range for the pumping pressure ratios was from 3 to 44.

It was found experimentally that the pumping fluid leaving the nozzle can evacuate its own environment to an approximate optimum value of 0.025 atmosphere. This minimum value (0.025 atmosphere) appears to be a function of pumping-fluid pressure and ejector-tube area ratio, provided the ejector tube has sufficient length. For ejectors not having sufficient length, the minimum value (different from the optimum) becomes a function of pumping-fluid pressure and ejector length-to-diameter ratio.

A model of the ejector flow phenomenon was deduced from experimental observations. From the model, a theory for obtaining ejector performance was developed. A comparison of the theory with experimental results is reported herein.

## INTRODUCTION

Rocket-ejector systems are of interest as a method for obtaining altitude performance of rocket engines. For example, references 1 and 2 present altitude performance of rocket engines where the expelled rocket

gases acted as the pumping fluid of the ejector system. This ejector method provided a simple and inexpensive apparatus for simulating altitude in comparison with the more expensive evacuated chambers, exhausters, or altitude wind-tunnel facilities. Therefore, an experimental and analytical study of the effects of ejector geometry on ejector performance was undertaken at the Lewis Research Center.

A literature survey showed many types of ejectors that utilized a low-pressure primary gas (pumping fluid). For example, cylindrical ejectors with a convergent nozzle are reported in references 3 and 4. The important ejector parameters reported in the literature were the length-to-diameter ratio of the ejector tube, the diameter ratio of ejector to primary nozzle, and the ratio of primary pressure to ejector ambient pressure. Upon completion of this survey it was felt that, if the kinetic energy of the primary gas could be increased by the use of a large-area-ratio DeLaval nozzle and high primary pressure, extremely low ejector pressures could be obtained for the same ejector-tube size. Therefore, a nonpumping ejector system consisting of a convergent-divergent nozzle enclosed by ejector tubes of constant area was used to study the important parameters influencing flow. High-pressure nitrogen gas was used as the primary fluid. The primary-nozzle area ratio of 9 was selected in order to avoid any possible gas condensation within the nozzle. Operation of the nozzle covered a range of primary pressure ratios from 3 to 44. Ejector tubes with length-to-diameter ratios from 2.67 to 12.0 were studied.

A theory for predicting performance of ejectors having cylindrical geometries was developed. The present report gives the experimental performance of the ejector system and the comparison with theory.

## SYMBOLS

A cross-sectional area

D diameter

L length

M Mach number

p static or total pressure

T total temperature

t static temperature

V velocity

$\gamma$ isentropic exponent

$\rho$ specific density

Subscripts:

a atmospheric

c chamber of primary fluid

e primary-nozzle exit

o ejector chamber

s separation plane in primary nozzle

t throat of primary nozzle

w ejector wall

1 station plane of primary-nozzle exit

2 station plane of shock attachment

3 station plane of ejector-tube exit

## APPARATUS AND PROCEDURE

### Apparatus

A schematic diagram of the ejector apparatus with defining nomenclature is shown in figure 1. The ejector system consisted of a primary chamber, a primary nozzle, a cylindrical ejector chamber, and an ejector tube. Four different ejector-tube geometries were employed.

The primary chamber was a 1.00-inch-diameter tube containing a straightening screen for the production of a uniform flow profile. Location of the primary-pressure tap was midway between the straightening screen and the primary-nozzle inlet.

The primary nozzle was designed to simulate a rocket nozzle with a $30^{\circ}$ half-angle convergent section, a 0.25-inch throat with 0.50-inch contour radius, and a $15^{\circ}$ half-angle divergent section with an exit diameter of 0.75 inch. These dimensions result in a nozzle area ratio of 9. A static-pressure tap was located at the nozzle exit in order to determine when the nozzle was under- or over-expanded.

The ejector chamber, which simulated the rocket-engine capsule of reference 1, was 2 inches in diameter with a length of 1.25 inches. This length resulted in 0.25-inch overlap from the end of the primary nozzle (see fig. 1). Two static-pressure taps were located in the ejector chamber for the purpose of determining whether any pressure gradients existed within the ejector chamber. The first pressure tap was located on the ejector-chamber wall, in the plane of the nozzle exit. The second pressure tap was located on the end wall of the ejector chamber (see fig. 1).

Four cylindrical ejector tubes were used. The inside tube diameters were 1.00, 1.25, 1.50, and 1.75 inches, with initial tube lengths of 12 inches. Each tube had 30 static-pressure taps arranged symmetrically along the length of the tube, as shown in figure 2.

Dry, high-pressure nitrogen gas acted as the primary fluid. The gas was supplied from a large reservoir at a pressure of 2800 pounds per square inch absolute; the pressure was then reduced by a control valve to the desired primary-chamber pressures. Care was taken to insure that no leaks resulting in secondary flow occurred in the ejector chamber.

## Instrumentation

All pressure measurements were made by mercury manometers except the primary-chamber pressure, which was measured by a Bourdon-tube pressure gage. All pressure recordings were photographed and then reduced from the photographic negatives.

## Procedure

The experimental investigation consisted of two parts. For the first part, data were obtained by varying primary-chamber pressure for each of the four ejector tubes and by holding the tube length constant. For the second part, data were obtained by varying primary-chamber pressure and tube length for the 1.50-inch-diameter ejector tube.

For each primary-chamber pressure, the following data were recorded: primary-chamber pressure, ejector-chamber pressures, primary-nozzle exit pressure, and ejector-tube wall pressures. Also recorded were the reference measurements of barometric pressure and manometer-board temperature. The manometer-board temperature was used in conjunction with reference 5 to obtain a correction for the manometer readings.

For most tests, the primary pressure was varied over a range in only one direction: from 3 to 44 atmospheres. For one test, the pressure was varied in both directions; and hysteresis, similar to that of references 3 and 4, was observed.

A reproducibility check was made on the data for the primary pressure varied in one direction only. The results indicated that reproducibility was within the measurement errors.

## RESULTS AND DISCUSSION



The effects of various dimensions of a nonpumping cylindrical-ejector system on the ejector-chamber pressure ratio $p_o/p_a$ for various primary-chamber pressure ratios $p_c/p_a$ were determined by theory and by experiment. Ejector-tube area ratio (ratio of cross-sectional area of ejector tube to throat of the primary nozzle $A_3/A_t$) and ejector-tube length-to-diameter ratio $L/D$ were studied. The primary-nozzle area ratio was held constant at a value of 9. This area ratio of 9 was chosen in order to eliminate the problem of gas condensation within the nozzle. No consideration was given to condensation occurring after the gas leaves the nozzle.

The results are presented by discussing first the theoretical performance, then the experimental performance, and finally the design parameters for minimum $p_o/p_a$.

### Theoretical Performance

A theory for ejector performance was developed for a flow model that conformed to experimental results (see appendix). The model is depicted in figure 3. The theory requires that the ejector tube be long enough for its exit to flow full. Assumptions for the theory included one-dimensional, nonviscous, adiabatic flow.

Experimental observation indicated that, as $p_c/p_a$ was increased from a low value, three distinct flow regimes were successively produced; these regimes are shown in figure 3. The first regime is defined as case I, in which the primary flow separates within the primary nozzle and the separation has initial and final limits at the nozzle throat and exit, respectively; the second regime, case II, has a starting limit when incipient separation occurs at the nozzle exit and an end limit when shock attachment exists at the ejector-tube exit; and the third regime, case III, begins with the end limit of case II and extends to all primary-chamber pressure ratios that produce internal shock attachments at the ejector-tube wall; the pressure rise across the shocks results in the ejector exit pressure being equal to the atmospheric pressure.

Theoretical results covering the range of experimental test conditions are presented in figure 4. Values of $p_o/p_a$ against $p_c/p_a$ are plotted for various $A_3/A_t$; also included are the limits of the three flow

regimes. The span between the initial and terminating limits, respectively, of cases I, II, and III covers regions of increasing $p_c/p_a$. As $p_c/p_a$ increases, $p_o/p_a$ decreases for cases I and II but increases for case III. When shock attachment begins, $p_o/p_a$ is a minimum (hereinafter called "minimum point"). The minimum point occurs at higher values of $p_c/p_a$ as $A_3/A_t$ increases, and the value of $p_o/p_a$ approaches zero asymptotically.

No attempt has been made in this report to theoretically optimize ejector performance with respect to primary-nozzle area ratio, ejector-tube area ratio, and ejector-tube length-to-diameter ratio. Hence, figure 4 shows in general the characteristic effects of $A_3/A_t$ on $p_o/p_a$ for various $p_c/p_a$.



## Experimental Performance

The experimental data are presented in three groups: (1) ejector performance, (2) primary-nozzle performance, and (3) ejector-tube wall pressure distributions.

Ejector performance. - The experimental and theoretical ejector performance curves for the 12-inch-length ejector tubes are given in figure 5(a). Plotted are the pressure parameters of $p_o/p_a$ against $p_c/p_a$ for area ratios $A_3/A_t$ from 16 to 49. It should be noted that tube length was constant; therefore, L/D varied from 12 to 6.86.

In general, figure 5(a) indicates that the experimental data were in reasonable agreement with theory. Between the starting limits of cases I and III, the agreement improved with larger values of $A_3/A_t$ except for $A_3/A_t$ of 49. This improvement is considered to be the result of attenuating the viscous and three-dimensional flow effects, but the departure from theory for $A_3/A_t$ of 49 is an L/D effect (discussed later herein). The agreement at the minimum points, starting limit of case III, also improved as $A_3/A_t$ increased; again, the exception was for $A_3/A_t$ of 49. Beyond the minimum point, the agreement was good for all values of $A_3/A_t$.

Figure 5(a) also indicates the existence of an audible flow instability (buzzing). This buzzing occurred while operating in the regime of case II and stopped at the end of case II. During buzzing, the manometers were not stable; hence, the data presented are averaged pressure readings. Once the minimum point was attained, the manometers were steady for all primary-chamber pressure ratios greater than, and including, the minimum point. Therefore, the value of $p_o/p_a$ at the minimum point should be reliable. For the $A_3/A_t$ investigated, this value was approximately constant at 0.025.

Performance of a constant-diameter ejector tube of various lengths is presented in figure 5(b). Test data covered a range of $L/D$ from 8.00 to 2.67 and a constant $A_3/A_t$ of 36. Results are plotted in terms of $p_o/p_a$ against $p_c/p_a$. Also presented is a theoretical curve for a long ejector tube with an $A_3/A_t$ of 36.

The experimental curves (fig. 5(b)) show the following general results: An increasing deviation from theory occurred as $L/D$ decreased; buzzing was observed for only two high values of $L/D$; the flow regime of case III was approached by a discontinuity (jump); and hysteresis was found. The $L/D$ effects indicate that for an $L/D$ of 8.00 the deviation from theory was least and the minimum point was approached through a buzzing region. For $L/D$ of 6.67, the deviation increased, and the same minimum point was approached by a jump and a buzz region. As $L/D$ decreased from 6.67 to 4.00, the deviation and jump became stronger, but buzzing was not observed; also, the flow regime of case III was approached without passing through the same minimum point as for larger $L/D$'s. When $L/D$ was 2.67, the jump did not exist, and the flow regime of case III was not attained.

The jumps, as well as buzzing, are related to the various kinds of flow that can occur in the system. An analysis of the flow stability conditions can be derived from the results of figure 5(b) and the theoretical requirement of sufficient ejector-tube length. When $L/D$ was large, such as 8.00, buzzing existed just before shock attachment occurred at the ejector-tube exit. (Buzzing can be deduced from the model and from theory to be an oscillatory movement of the shock attachment point from the nozzle exit to the ejector-tube exit.) When $L/D$ was 6.67, the first jump phenomenon with buzzing was observed. Such jumps may result from unsteady flow at the tube exit. This explanation of jump and buzz is based on the fact that, before the jump occurred, the data deviated markedly from theory; this would indicate that the ejector was not flowing full at the exit. Therefore, buzzing was not of the same form as for $L/D$ of 8.00, where the deviation from theory was slight. When $L/D$ was 5.33 or 4.00, a rapid jump occurred with a slight increase in $p_c/p_a$. This transition did not result in buzzing. The stability of flow in these cases was probably due to the magnitude of $p_c/p_a$ and the resulting shock location. Finally, for $L/D$ of 2.27, the ejector-tube did not flow full for the $p_c/p_a$ range investigated; but, if the range were increased sufficiently, operation similar to that for the $L/D$ of 4.00 would be obtained.

The effects of hysteresis on ejector performance were studied for an $L/D$ of 4.00 only; results are presented in figure 5(b). Hysteresis was investigated by first increasing and then decreasing $p_c/p_a$. The effect of hysteresis was the attainment of a lower $p_o/p_a$ value than that produced by the initial jump. The actual hysteresis path was not determined.

A cross interpretation of figures 5(a) and (b) provides a study of L/D effects on $A_3/A_t$, reproducibility of measurements, and methods of altitude simulation for rocket engines.

The L/D effects are obtained by comparing the curves for L/D of 6.67 in figure 5(b) with an approximately equal L/D of 6.86 in figure 5(a). The deviation from theory for both curves is observed to be similar in characteristics. This similarity justifies the statement made during the discussion of figure 5(a) that the deviation from theory for $A_3/A_t$ of 49 was an L/D effect. Also, the deviation from theory at the minimum point could be less if a larger L/D were used. Finally, a conclusion may be made from figure 5(b) that, if an $A_3/A_t$ greater than 49 were used for the pressure range of figure 5(a), then the ejector tube either would not flow full or would encounter a jump.

An example of the reproducibility of measurements for the same ejector tubes can be obtained by comparing the experimental curve for $A_3/A_t$ of 36 in figure 5(a) with the experimental curve for L/D of 8 in figure 5(b). It is felt that the comparison is valid and shows the reproducibility of data to be within measurement errors.

Three methods for altitude simulation for rocket engines can be derived from the results of figure 5. These methods require that the rocket-ejector system operate in the flow regime of case III, which in turn requires the nozzle to flow full and shock attachment to exist. The first method is one in which an $A_3/A_t$ curve is followed as $p_c/p_a$ is varied, whereas the second method is one in which different points on $A_3/A_t$ curves are obtained by fixing $p_c/p_a$. Hysteresis suggests the third method of operation. For example, if the requirement of ejector-tube length is critical, a limited range of rocket-engine altitude performance can be obtained by overpressurizing the rocket chamber until shock attachment is established. Then, decreasing the rocket-chamber pressure would result in higher altitude conditions until the left end point of the hysteresis loop is reached.

Lower altitude simulation may be obtained by operating the ejector system in flow regimes other than case III. These methods utilize the same variation technique as the first and second methods. The methods encompass long as well as short ejector tubes, and the operation is restricted to regions other than buzzing. The rocket-engine performance measured at these lower altitudes may be valid provided the boundary-layer feedback along the ejector-tube wall has little effect on the internal rocket-nozzle boundary layer or flow separation.

Primary-nozzle behavior. - The behavior of the primary-nozzle exit pressure is presented in figure 6. The primary-nozzle exit pressure ratio $p_e/p_a$ is plotted against $p_c/p_a$. Also presented is a theoretical

curve based on one-dimensional isentropic flow, a specific-heat ratio of 1.40, and a 9:1-area-ratio nozzle flowing full. Figure 6(a) considers constant-length ejector tubes of various $A_3/A_t$, whereas figure 6(b) is for a constant-diameter ejector-tube with varying L/D. Both figures show data recorded during buzz, and figure 6(b) gives the hysteresis data.

The general characteristics of the experimental curves shown in figures 6(a) and (b) are similar in that $p_e/p_a$ descends and then rises linearly as $p_c/p_a$ increases. Data recorded during the linear rise are in good agreement with theory; therefore, the primary nozzle must be flowing full. From the descending data, it can be concluded that the nozzle first encountered flow separation for low values of $p_c/p_a$ and then a shock wave at the nozzle exit for higher $p_c/p_a$. The ranges of $p_c/p_a$ for these two flow conditions can be obtained from the limits of cases I and II.

For a fixed low value of $p_c/p_a$, figure 6(a) shows that $p_e/p_a$ increased with an increase in $A_3/A_t$. Figure 6(b) shows the same effect with a decrease in L/D. These results indicate a conclusion; that is, the point of flow separation moves toward the throat of the nozzle. Also, observations indicate that buzzing had no effect on nozzle exit pressure except for $A_3/A_t$ of 16 but that hysteresis had a small influence on this pressure.

Ejector wall pressure distributions. - The ejector-tube-wall and the ejector-chamber pressure distributions for constant-length ejector tubes are shown in figure 7 for various ejector-tube area ratios and varying $p_c/p_a$. The pressures are plotted against the longitudinal positions of the pressure tap. Not all of the pressure distributions corresponding to data points in figure 5 are presented; part of the data was deleted for clarity. Also deleted were the pressure distributions for the buzzing condition, since these data would be questionable because of instability.

Figure 7 shows that, for any constant value of $p_c/p_a$, pressure gradients did not exist within the ejector chamber. Zero gradients conveniently result in simplification of thrust measurements when an ejector is used to simulate altitude with the rocket engine acting as the primary nozzle.

In general, the ejector-wall gradients are similar in all parts of figure 7. For discussion of generalities, consider figure 7(a). The ejector-chamber results indicate that, as $p_c/p_a$ increased, the environmental pressure $p_o$ continually dropped until the shock attached to the wall near the nozzle region of the ejector tube; a further increase in

$p_c/p_a$ gave an increase in $p_o$. The ejector-tube wall pressure distributions show that: (1) The ejector-tube exit pressure equaled the atmospheric pressure for all $p_c/p_a$; (2) for low values of $p_c/p_a$, the wall pressure distributions were smooth and continually increased in slope; (3) as $p_c/p_a$ was further increased, Prandtl-Meyer expansion occurred about the primary-nozzle exit plane and caused a discernible attached shock pattern to exist within the ejector tube; (4) the number of shock patterns increased with increasing $p_c/p_a$; and (5) the number and strength of these shock patterns decreased with increasing $A_3/A_t$ (see figs. 7(a) to (d)).

The ejector-tube-wall and the ejector-chamber pressure distributions for constant-diameter tubes having various L/D are presented in figure 8. A comparison of figures 7 and 8 reveals a similarity in pressure distributions. An exception to the similarity occurs in parts (d) and (e) of figure 8; the ejector-tube exit pressure did not attain the value of atmospheric pressure, and part (e) does not show a discernible shock pattern.

## Design Parameters for Minimum Point

As an aid toward ejector design, figure 9 is presented. This figure is a composite plot of $p_c/p_a$ against $p_c/p_o$, $p_c/p_o$ against $p_e/p_o$, and $p_e/p_o$ against $A_3/A_t$. These parameters were selected as design criteria because they combine ejector dimensions with rocket-engine nozzle parameters. The curves were obtained for the minimum points of the theoretical and experimental data presented in figures 4, 5(a), and 6(a). These curves apply only for ejector tubes of sufficient length and a primary-nozzle area ratio of 9. A figure similar to figure 9 can be obtained from the data of figures 5(b) and 6(b) for ejector designs when tube length becomes a critical parameter because of space limitations. Also, similar theoretical curves for primary-nozzle area ratios other than 9 can be calculated from the theory presented in the appendix.

The use of figure 9 is explained by following the dashed guide line. For example, given a rocket engine with a nozzle area ratio of 9 and a sea-level pressure ratio of 25. Entering figure 9 with $p_c/p_a$ of 25 gives an altitude pressure ratio $p_c/p_o$ for the nozzle of 940 and a nozzle-exit back-pressure ratio $p_e/p_o$ of 7.7. The pressure ratio of 25 results in an ejector with an area ratio $A_3/A_t$ of 32.5.

Figure 9 does not consider the effects of primary fluid temperature and specific heat ratio on ejector performance. These parameter effects can be obtained from references 4 and 6.

E-483

CH-2 back

## SUMMARY OF RESULTS

The following results were obtained from a theoretical and experimental investigation of a nonpumping ejector system utilizing cylindrical ejector tubes of various length-to-diameter ratios:

1. The theoretical values obtained by employing the equations of energy, momentum, and conservation of mass were in good agreement with the corresponding experimental values for long ejector tubes.

2. For large ratios of primary-chamber pressure to ejector-tube back pressure (primary pressure ratio) and for adequate ratios of ejector-tube length to diameter, the expanding primary jet attached to the ejector-tube wall and established shock patterns within the ejector tube. The static pressure of the expanded flow before the initial attached shock wave can be approximated by assuming that it is a function of the ejector-tube to nozzle-throat diameter ratio only.

3. For small primary pressure ratios, the primary nozzle encountered flow separation. The performance of the ejector was affected by flow separation and could be adequately explained by use of the developed theory, which utilized empirical data for nozzle flow separation.

4. The results indicate a useful means of obtaining a limited range of rocket-engine altitude performance by incorporating the rocket engine as the primary nozzle of an ejector system.

Lewis Research Center
National Aeronautics and Space Administration
Cleveland, Ohio, October 8, 1959

## APPENDIX - EJECTOR THEORY; NO SECONDARY FLOW AND SUFFICIENTLY LARGE LENGTH-TO-DIAMETER EJECTOR-TUBE RATIOS

The experimental data of the ejector system showed that the primary nozzle encountered flow separation at low primary pressure ratios. As the primary pressure ratio increased, the flow filled the nozzle at a pressure ratio corresponding to the design area ratio. Further increase in primary pressure ratio resulted in Prandtl-Meyer expansion about the nozzle exit. The expanded flow produced a discernible shock pattern within the ejector tube and (for all practical purposes) a linear variation of ejector pressure ratio with increasing primary pressure ratio. The experimental wall-pressure distributions of the ejector tube indicated that the ejector exit pressure was identical to the atmospheric pressure. These phenomena were also apparent from pressure measurements and from shadowgraphs in reference 7.

From the experimental observations, a flow model was proposed and is shown in figure 3. The discussion of the model and the flow regimes (cases I, II, and III) is presented in the RESULTS AND DISCUSSION section. With the aid of the model, theoretical equations were developed from the following assumptions:

(1) No friction or shear forces in ejector tube

(2) Adiabatic flow, $T_c = T_s = T_e = T_2 = T_3$

(3) $p_3 = p_a$

(4) Constant-area duct

(5) Ideal gas law holds; no gas condensation

(6) Primary-nozzle flow is isentropic up to separation point

(7) Primary fluid fills ejector-tube exit

### Case I, Flow Separation in Primary Nozzle

By applying one-dimensionality, the equations for continuity, energy, and momentum can be expressed between the nozzle flow-separation point and the end of the ejector tube.

The continuity equation can be written as

$$\rho_s A_s V_s = \rho_3 A_3 V_3$$

or by use of ideal gas law, the definition of Mach number, and $p_3$ equals $p_a$,

$$\frac{p_s A_s M_s}{\sqrt{t_s}} = \frac{p_a A_3 M_3}{\sqrt{t_3}} \tag{A1}$$

From the energy equation and the assumption of adiabatic flow, the total temperature can be expressed as

$$T_c = t_s\left(1 + \frac{\gamma - 1}{2} M_s^2\right) = t_3\left(1 + \frac{\gamma - 1}{2} M_3^2\right) \tag{A2}$$

Substitution of $t_s/t_3$ from equation (A2) into equation (A1) yields the continuity equation in the following form:

$$\left(\frac{p_s A_s M_s}{p_a A_3}\right)^2 \left(1 + \frac{\gamma - 1}{2} M_s^2\right) = M_3^2 + \frac{\gamma - 1}{2} M_3^4$$

Solving for $M_3^2$ by applying the quadratic formula gives

$$M_3^2 = \frac{-1 \pm \sqrt{1 + 2(\gamma - 1)\left(\frac{p_s M_s A_s}{p_a A_3}\right)^2 \left(1 + \frac{\gamma - 1}{2} M_s^2\right)}}{\gamma - 1} \tag{A3}$$

Equation (A3) shows that, for $\gamma > 1$ and $M_3$ not imaginary,

$$M_3^2 = \frac{-1 + \sqrt{1 + 2(\gamma - 1)\left(\frac{p_s M_s A_s}{p_a A_3}\right)^2 \left(1 + \frac{\gamma - 1}{2} M_s^2\right)}}{\gamma - 1} \tag{A4}$$

When assumptions (1), (3), (4), and (5) are incorporated, the equation for conservation of momentum across the flow-separation plane and the ejector-tube exit can be expressed as

$$\frac{p_o}{p_s}\left(\frac{A_3}{A_s} - 1\right) + 1 - \frac{p_a}{p_s}\frac{A_3}{A_s} = \gamma \frac{p_a}{p_s}\frac{A_3}{A_s} M_3^2 - \gamma M_s^2 \tag{A5}$$

Substitution of $M_3^2$ from equation (A4) into equation (A5) results in the following form for the conservation of momentum:

$$\left(\frac{p_a}{p_s}\right)^2\left(\frac{A_3}{A_s}\right)^2\left(\frac{\gamma+1}{\gamma-1}\right) - \frac{p_a}{p_s}\frac{2A_3}{(\gamma-1)A_s}\left[\frac{p_o}{p_s}\left(\frac{A_3}{A_s}-1\right)+1+\gamma M_s^2\right]$$

$$+\frac{2\gamma^2}{\gamma-1}M_s^2\left(1+\frac{\gamma-1}{2}M_s^2\right) - \left[\frac{p_o}{p_s}\left(\frac{A_3}{A_s}-1\right)+1+\gamma M_s^2\right]^2 = 0$$

Letting

$$a = \left(\frac{A_3}{A_s}\right)^2\left(\frac{\gamma+1}{\gamma-1}\right)$$

$$b = -\frac{2}{\gamma-1}\frac{A_3}{A_s}\left[\frac{p_o}{p_s}\left(\frac{A_3}{A_s}-1\right)+1+\gamma M_s^2\right]$$

$$c = \frac{2\gamma^2}{\gamma-1}M_s^2\left(1+\frac{\gamma-1}{2}M_s^2\right) - \left[\frac{p_o}{p_s}\left(\frac{A_3}{A_s}-1\right)+1+\gamma M_s^2\right]^2$$

and applying the quadratic formula for $p_a/p_s$ result in

$$\frac{p_a}{p_s} = \frac{-b \pm \sqrt{b^2-4ac}}{2a} \qquad \text{(A6)}$$

Equation (A6) requires knowledge of the functional relation of $A_3/A_s$, $p_o/p_s$, and $M_s$. Green (ref. 8) presented data on flow-separation pressure ratio $p_o/p_s$ for 15° half-angle rocket nozzles as a function of the rocket-nozzle pressure ratio $p_c/p_o$. For a given primary-nozzle area ratio, with the use of Green's data and the isentropic supersonic tables of reference 9 for $\gamma = 1.4$, equation (A6) may be solved in the following manner:

(1) Determine the primary-nozzle pressure ratio that results in incipient flow separation at the primary-nozzle exit. For this condition, $p_c/p_s$ equals $p_c/p_e$. By the use of Green's data, a cross plot of $p_c/p_s$ against $p_c/p_o$ can be obtained. The incipient flow-separation condition ($p_s = p_e$) and the fixed-nozzle area ratio will determine the limit of equation (A6), since incipient flow separation requires that $p_o/p_s > 1$.

(2) Assume various values of $M_s \leq M_e$ and obtain from reference 9 $A_t/A_s$ and $p_c/p_s$. By using Green's data for a cross plot of $p_o/p_s$ against $p_c/p_s$, obtain a value of $p_o/p_s$.

(3) By fixing $A_3$, compute

(a) $\frac{A_3}{A_s} = \frac{A_3}{A_t}\frac{A_t}{A_s}$

(b) a, b, and c

(c) $\frac{p_a}{p_s} = \frac{-b \pm \sqrt{b^2 - 4ac}}{2a}$

(d) $\frac{p_o}{p_a} = \frac{p_s}{p_a}\frac{p_o}{p_s}$

and

$\frac{p_c}{p_a} = \frac{p_c}{p_s}\frac{p_s}{p_a}$

(4) Equation (A6) results in double roots. The negative roots have negative values of $p_o/p_a$ and $p_c/p_a$ that are physically impossible. The positive root for $p_o/p_a > 1$ is also physically impossible.

Case II, Primary Nozzle Flowing Full

For the primary nozzle flowing without separation, equation (A4) can be modified and expressed as

$$M_3^2 = \frac{-1 + \sqrt{1 + 2(\gamma - 1)\left(\frac{p_e}{p_a}\frac{A_e M_e}{A_3}\right)^2\left(1 + \frac{\gamma - 1}{2}M_e^2\right)}}{\gamma - 1}$$

But $\frac{p_e}{p_a} = \frac{p_c}{p_a}\frac{p_e}{p_c}$; and, for a fixed-primary-nozzle area ratio, $M_e$ and $p_e/p_c$ are constant for a given $\gamma$. Therefore,

$$M_3^2 = \frac{-1 + \sqrt{1 + A\left(\frac{p_c}{p_a}\frac{A_e}{A_3}\right)^2}}{B} \qquad \text{(A7)}$$

where

$$A = 2(\gamma - 1)\left(\frac{p_e}{p_c}\right)^2 M_e^2\left(1 + \frac{\gamma - 1}{2} M_e^2\right)$$

$$B = \gamma - 1$$

The conservation of momentum applied between the primary-nozzle exit and the ejector-tube exit can be expressed as

$$\frac{p_o}{p_a}\left(\frac{A_3}{A_e} - 1\right) + \frac{p_e}{p_a} - \frac{A_3}{A_e} = \gamma \frac{A_3}{A_e} M_3^2 - \gamma \frac{p_e}{p_a} M_e^2$$

Again, for a fixed primary nozzle, constant $\gamma$, and the substitution of equation (A7) into the preceding equation, the result is:

$$\frac{p_o}{p_a} = \frac{\frac{A_3}{A_e}\left\{1 + \gamma \frac{\left[-1 + \sqrt{1 + A\left(\frac{p_c}{p_a}\frac{A_e}{A_3}\right)^2}\right]}{B}\right\}}{\frac{A_3}{A_e} - 1} - \frac{\frac{p_c}{p_a} C}{\frac{A_3}{A_e} - 1} \qquad \text{(A8)}$$

where

$$C = \frac{p_e}{p_c}(1 + \gamma M_e^2)$$

Equation (A8) gives the ejector pressure ratio only as a function of the primary pressure ratio for a fixed-primary-nozzle area ratio, ejector-tube diameter, and a constant gamma. Therefore, by fixing the primary-nozzle area ratio and assuming primary-ejector pressure ratios $p_c/p_a$, values of $p_o/p_a$ are obtained for various ejector-tube diameters.

## Case III, Prandtl-Meyer Expansion

Free expansion assumes that the flow fills the ejector at station 2 and that an attached shock pattern results initially at the ejector-tube exit. An infinitesimal distance ahead of the attachment point, isentropic flow exists. The assumption is made that the flow is one-dimensional and that the value of $p_o$ will be equal to the static pressure of the streamline for a free expansion to an area ratio of $A_3/A_t$. This condition results in a constant $p_o/p_c$. Therefore, $\frac{p_o}{p_a} = \frac{p_o}{p_c}\frac{p_c}{p_a}$;

this is a linear function in terms of $p_c/p_a$ because $p_o/p_c$ remains constant for a fixed $A_3/A_t$.

## Summary

The theoretical behavior of the ejector for various $A_3/A_t$ is summarized in figure 4. A comparison of the theory with experimental results is shown in figure 5 and is discussed in the RESULTS AND DISCUSSION section.

E-485

## REFERENCES

1. Fortini, Anthony, Hendrix, Charles D., and Huff, Vearl N.: Experimental Altitude Performance of JP-4 Fuel and Liquid-Oxygen Rocket Engine with an Area Ratio of 48. NASA MEMO 5-14-59E, 1959.

2. Hagginbothom, William K., Jr.: Straight-Pipe Diffuser Thruststand for Measuring High Altitude Rocket Performance. Paper presented at Joint Army-Navy-Air Force Solid Propellant Rocket Static Test Panel meeting, Sacramento (Calif.), Oct. 28-30, 1958.

3. Kochendorfer, Fred D., and Rousso, Morris D.: Performance Characteristics of Aircraft Cooling Ejectors Having Short Cylindrical Shrouds. NACA RM E51E01, 1951.

4. Kochendorfer, Fred D.: Effects of Properties of Primary Fluid on Performance of Cylindrical Shroud Ejectors. NACA RM E53L24a, 1954.

5. Marks, Lionel S.: Mechanical Engineers' Handbook. Fourth ed., McGraw-Hill Book Co., Inc., 1941.

6. Wood, Richard D.: Theoretical Ejector Performance and Comparison with Experimental Results. TR 54-556, WADC, Aug. 1954.

7. Fabri, J., and Paulon, J.: Theory and Experiments on Supersonic Air-to-Air Ejectors. NACA TN 1410, 1958.

8. Green, Leon, Jr.: Flow Separation in Rocket Nozzles. Jour. Am. Rocket Soc., vol. 23, no. 1, Jan.-Feb. 1953, pp. 34-35.

9. Ames Research Staff: Equations, Tables, and Charts for Compressible Flow. NACA Rep. 1135, 1953. (Supersedes NACA TN 1428.)

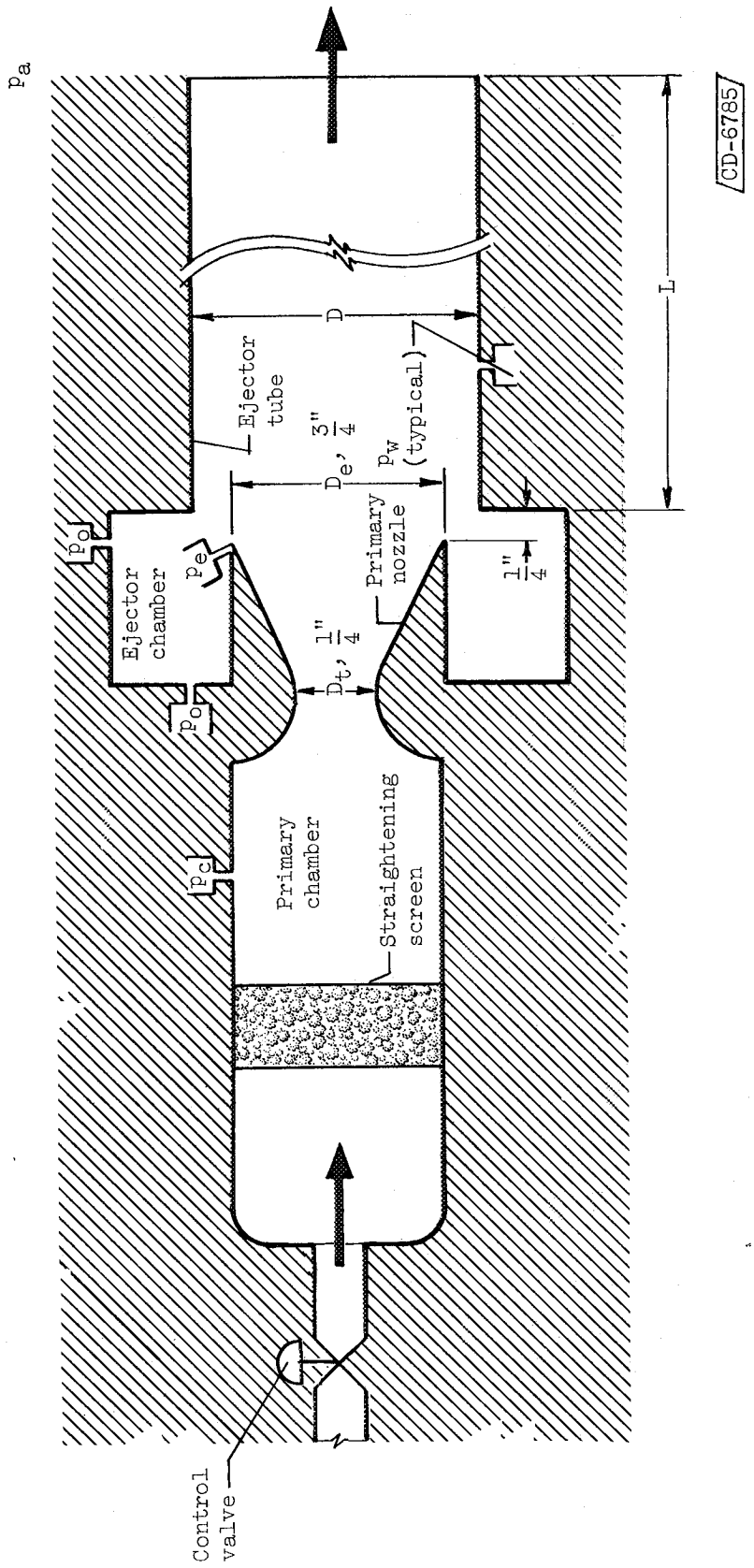


Figure 1. - Ejector system.

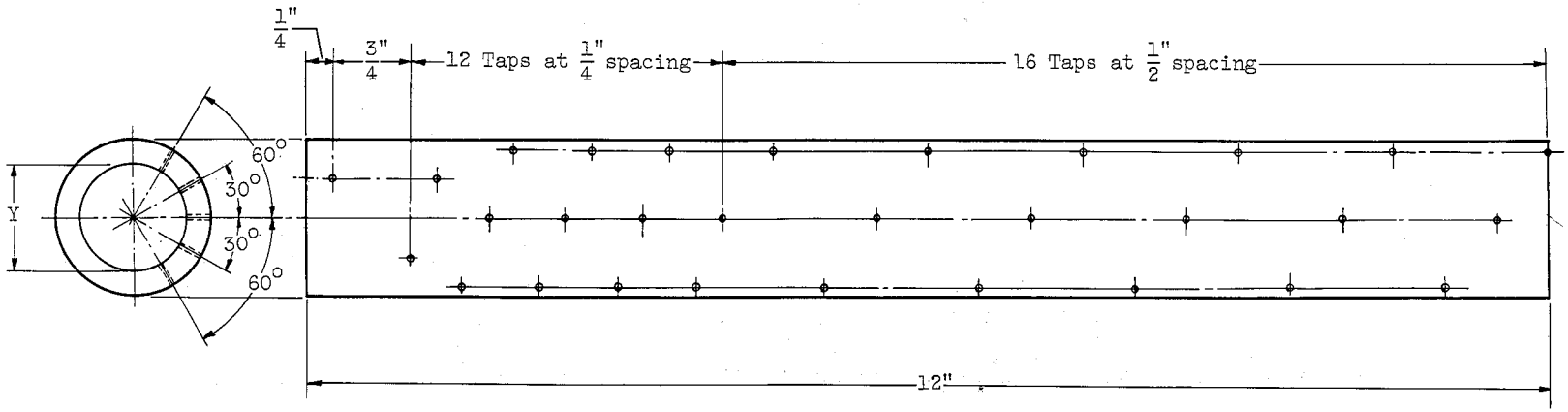


| Y-ejector tube I.D., in. |
|---|
| 1.00 |
| 1.25 |
| 1.50 |
| 1.75 |

Figure 2. - Ejector tubes with wall-pressure-tap locations.

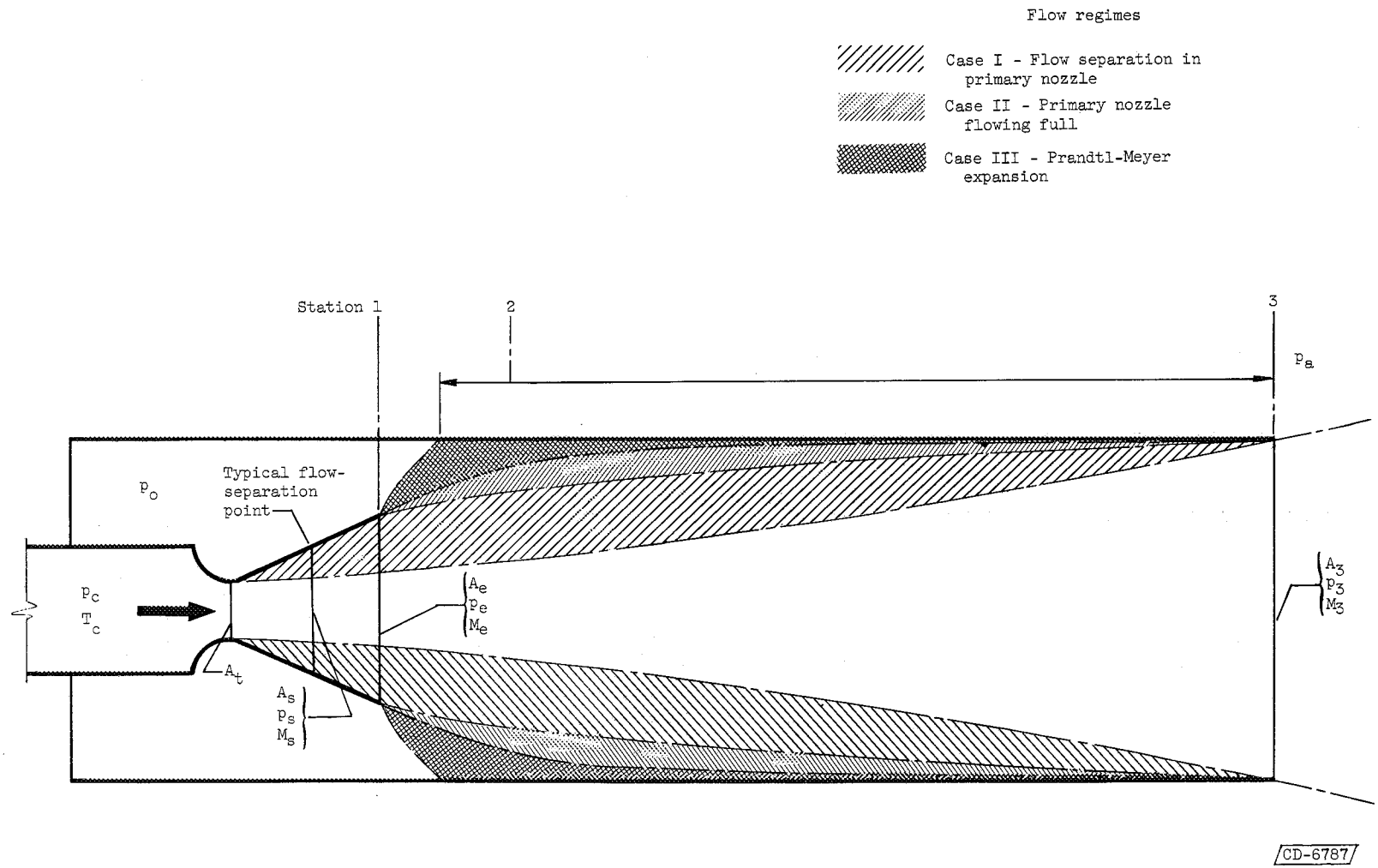


Figure 3. - Ejector flow model; no secondary flow.

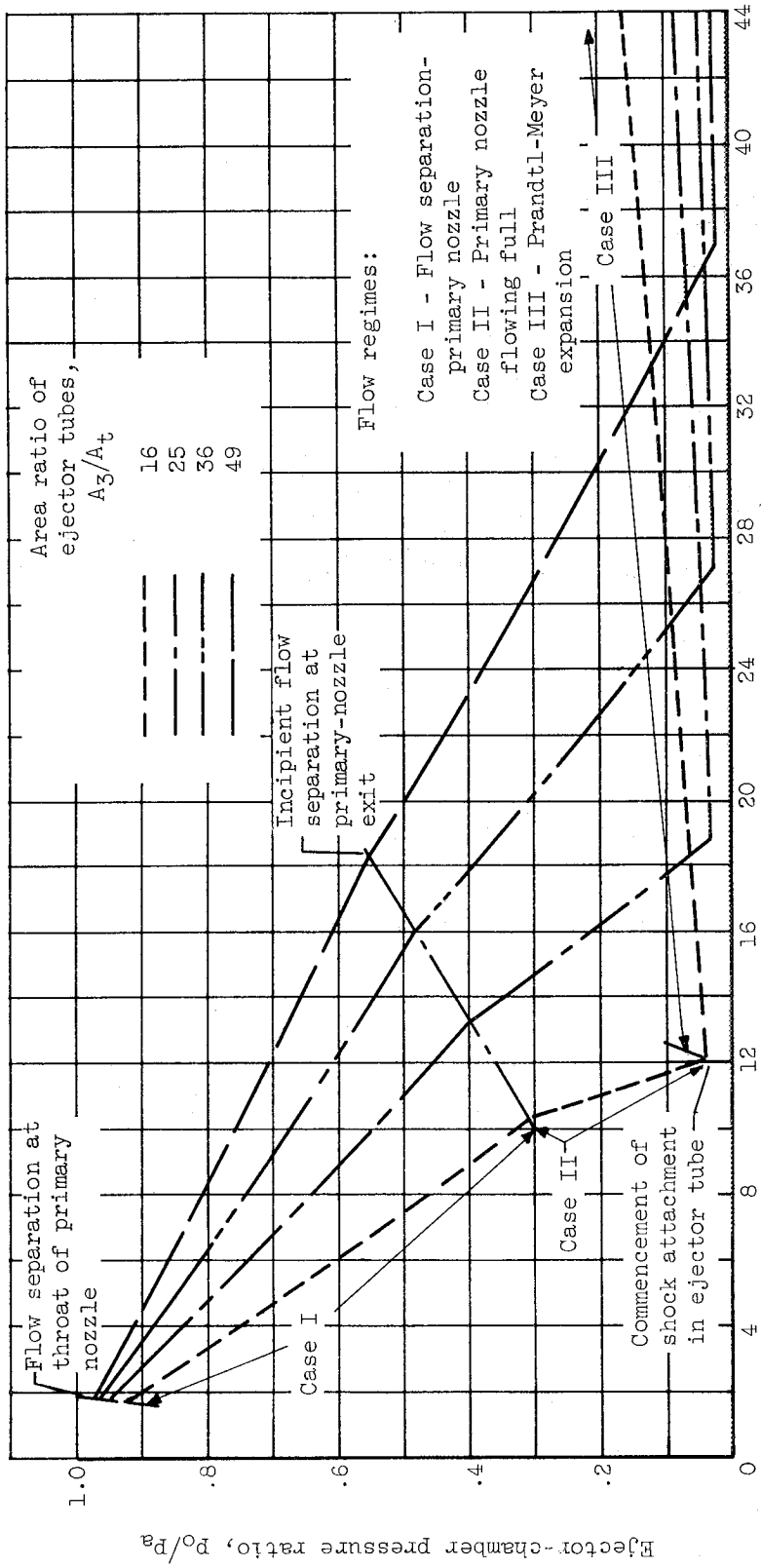


Figure 4. - Theoretical performance curves for cylindrical ejector tubes of sufficient length. Primary-nozzle area ratio, 9; no secondary flow.

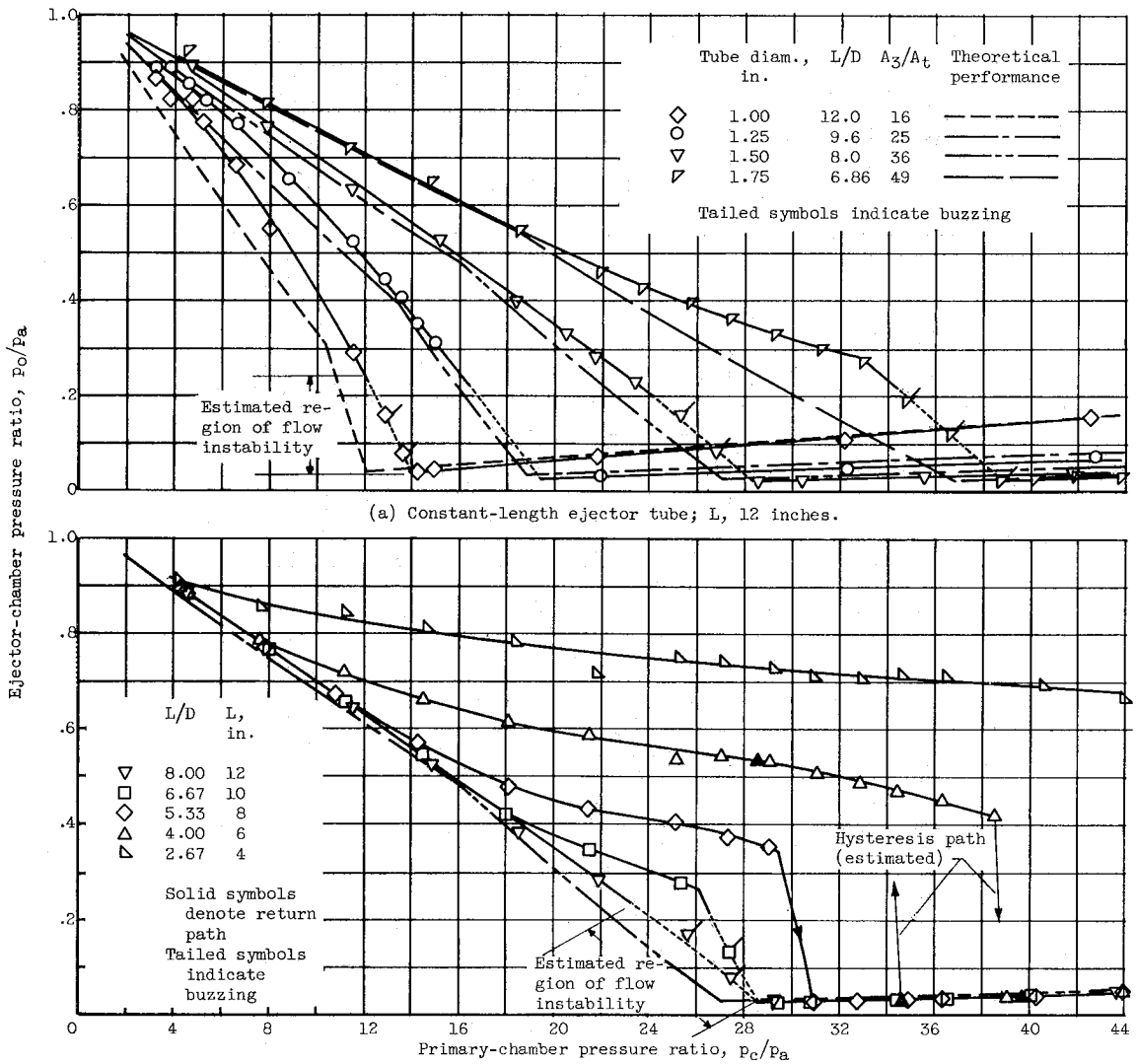


(a) Constant-length ejector tube; L, 12 inches.

(b) Constant-diameter ejector tube; D, 1.50 inches; $A_3/A_t$, 36.

Figure 5. - Experimental and theoretical performance of cylindrical ejector for various $A_3/A_t$ and L/D. Primary-nozzle area ratio, 9; no secondary flow.

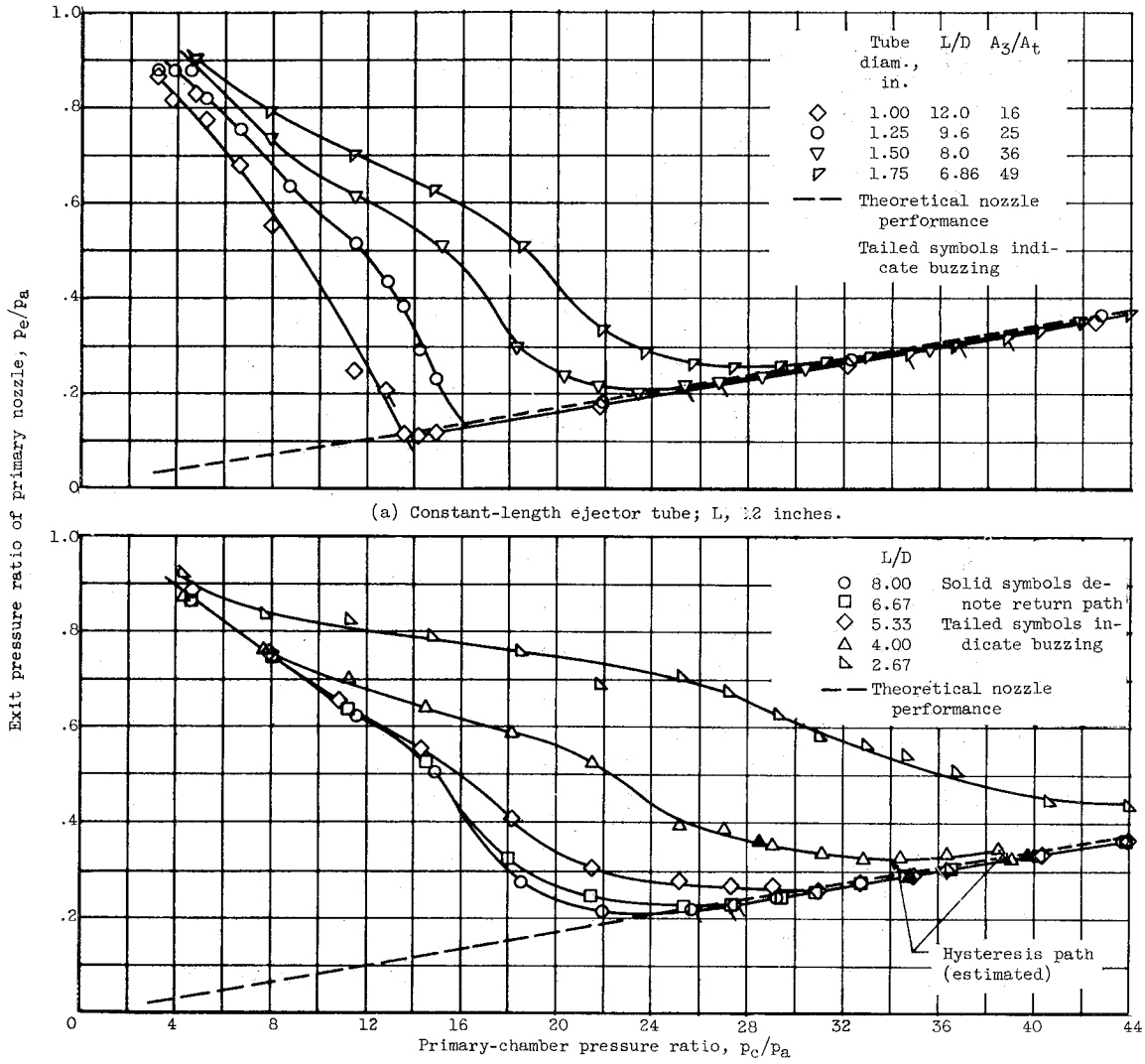


(a) Constant-length ejector tube; L, 12 inches.

(b) Constant-diameter ejector tube; D, 1.50 inches.

Figure 6. - Experimental and theoretical performance of ejector primary nozzle for ejectors of various $A_3/A_t$ and L/D. Primary-nozzle area ratio, 9; no secondary flow.

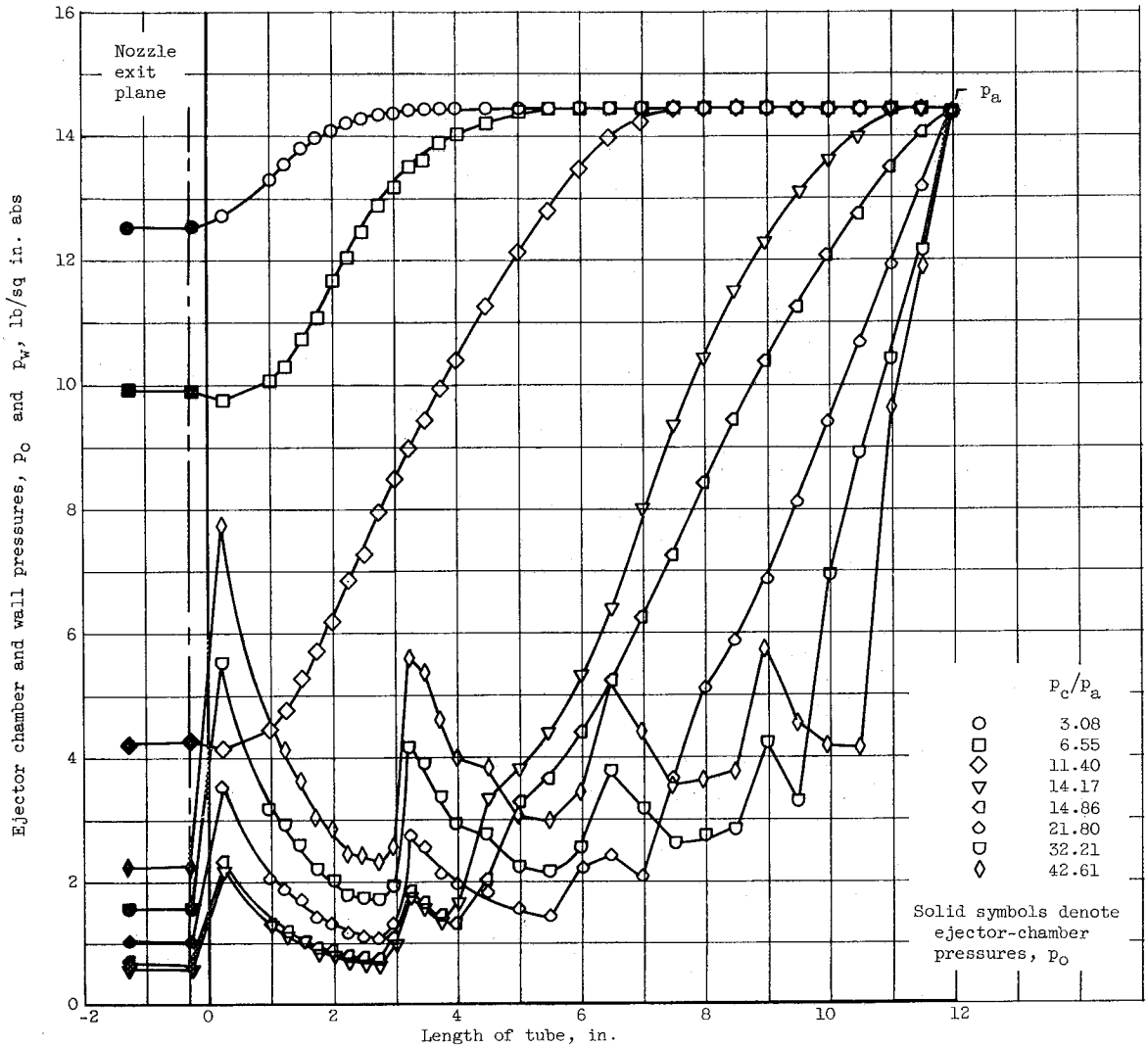


(a) 1.00-Inch-diameter ejector tube; $A_3/A_t$, 16.

Figure 7. - Ejector chamber and wall pressure distributions for constant-length ejector tubes having various $A_3/A_t$. Primary-nozzle area ratio, 9; no secondary flow.

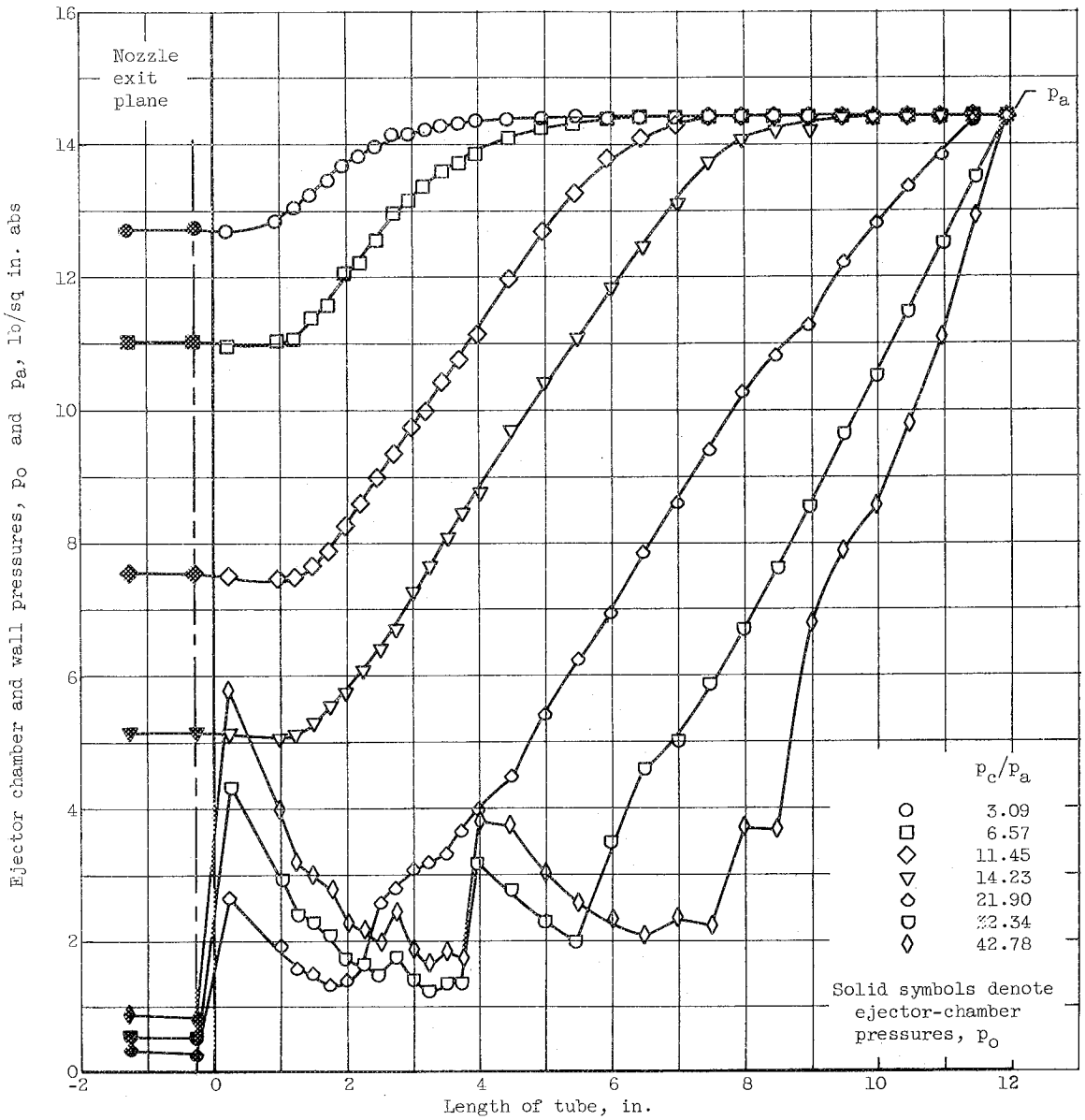


(b) 1.25-Inch-diameter ejector tube; $A_3/A_t$, 25.

Figure 7. - Continued. Ejector chamber and wall pressure distributions for constant-length ejector tubes having various $A_3/A_t$. Primary-nozzle area ratio, 9; no secondary flow.

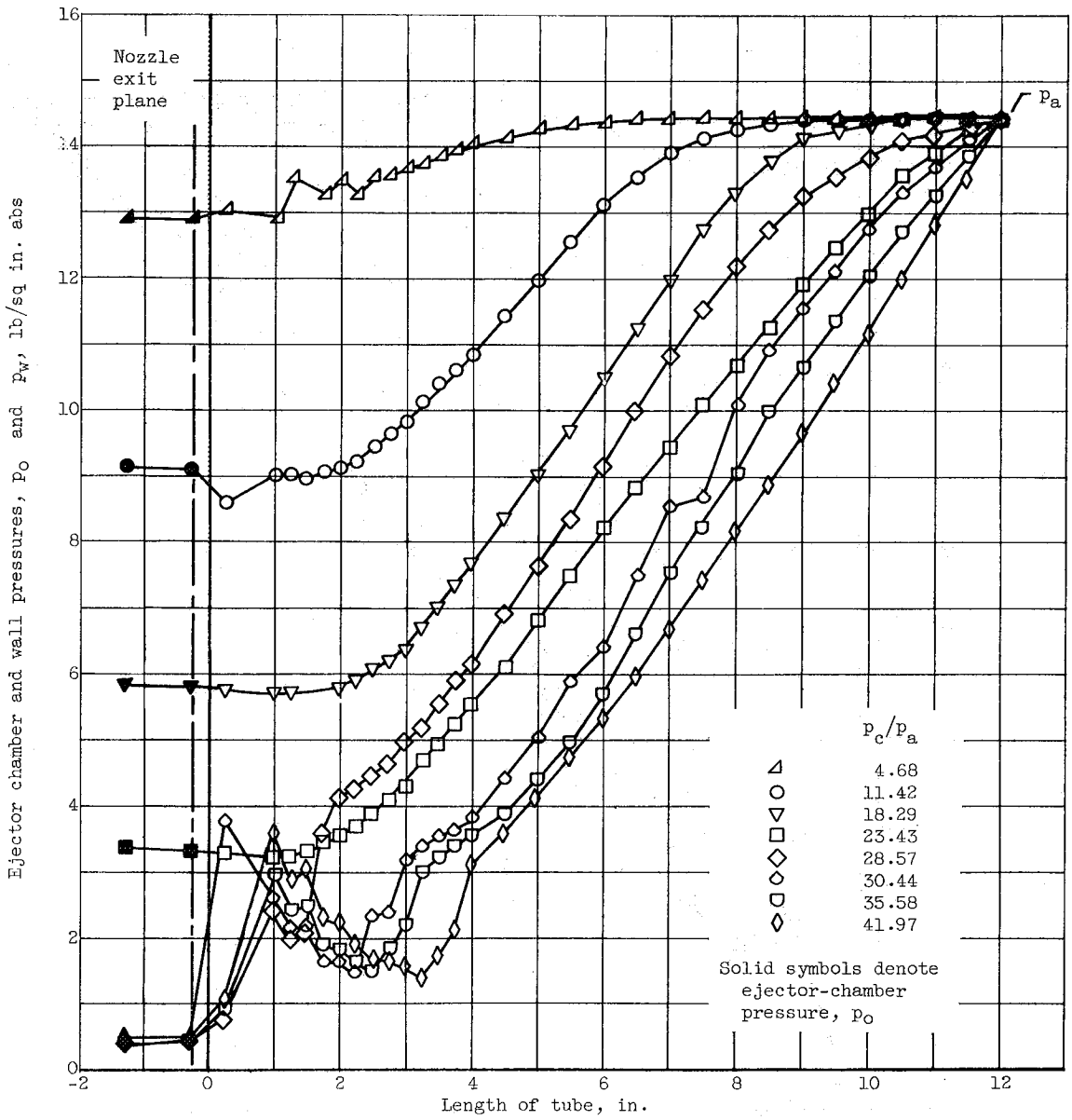


(c) 1.50-Inch-diameter ejector tube; $A_3/A_t$, 36.

Figure 7. - Continued. Ejector chamber and wall pressure distributions for constant-length ejector tubes having various $A_3/A_t$. Primary-nozzle area ratio, 9; no secondary flow.

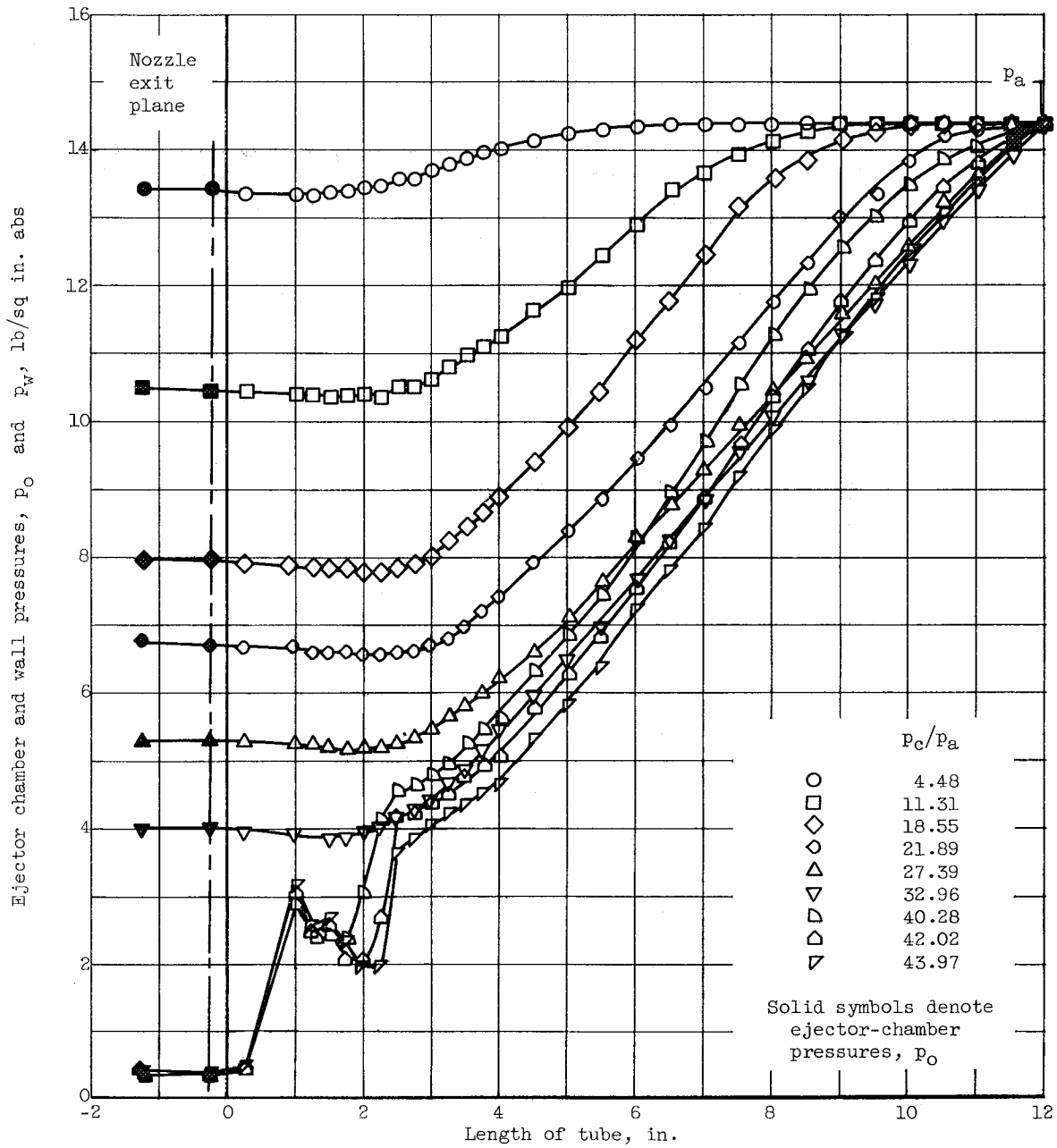


(d) 1.75-Inch-diameter ejector tube; $A_3/A_t$, 49.

Figure 7. - Concluded. Ejector chamber and wall pressure distributions for constant-length ejector tubes having various $A_3/A_t$. Primary-nozzle area ratio, 9; no secondary flow.

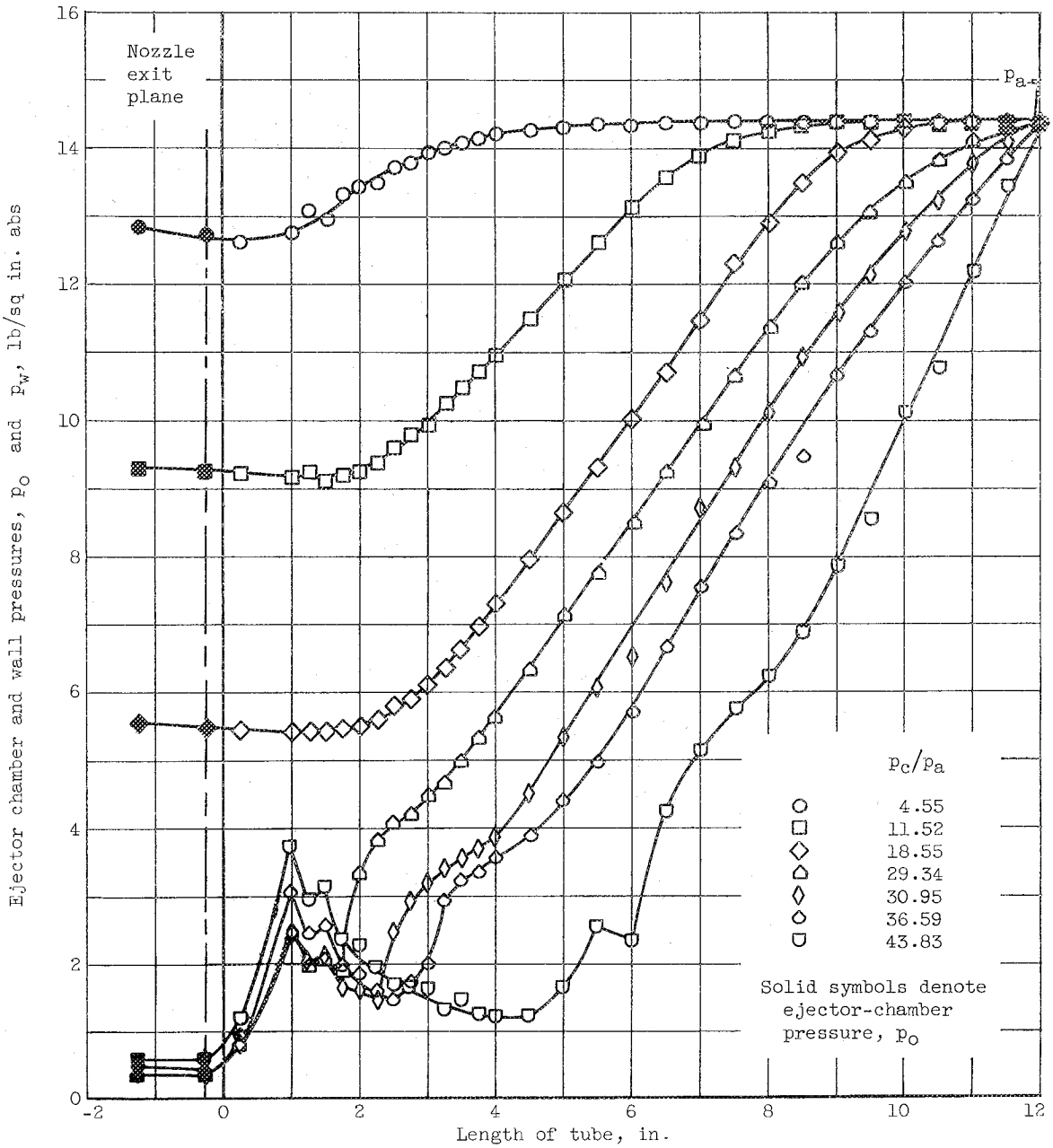


(a) L/D, 8.00; D, 1.5 inches.

Figure 8. - Ejector chamber and wall pressure distributions for constant-diameter ejector tubes having various L/D. Ejector-tube area ratio, $A_3/A_t$, 36; primary-nozzle area ratio, 9; no secondary flow.

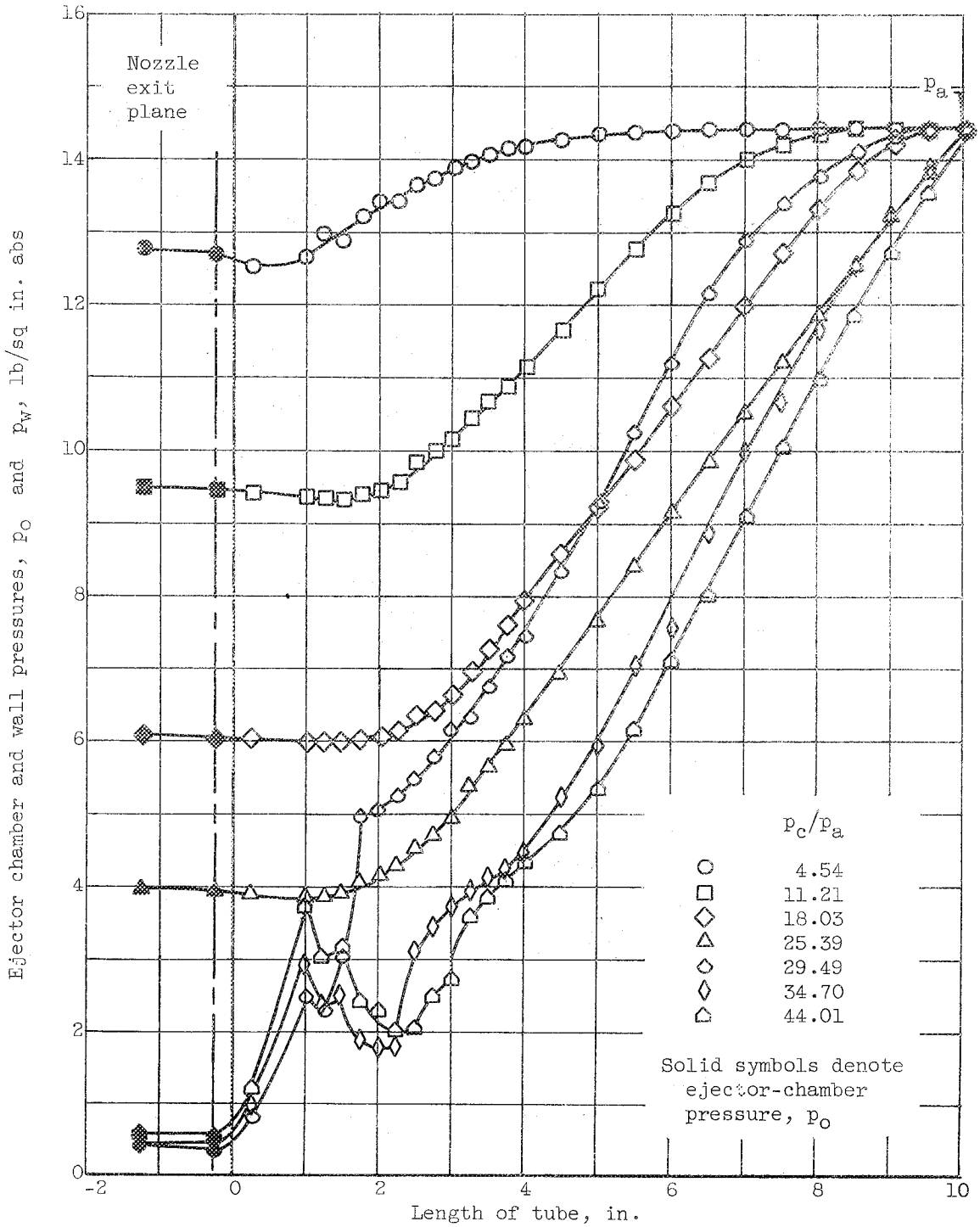


(b) L/D, 6.67; D, 1.5 inches.

Figure 8. - Continued. Ejector chamber and wall pressure distributions for constant-diameter ejector tubes having various L/D. Ejector-tube area ratio, $A_3/A_t$, 36; primary-nozzle area ratio, 9; no secondary flow.

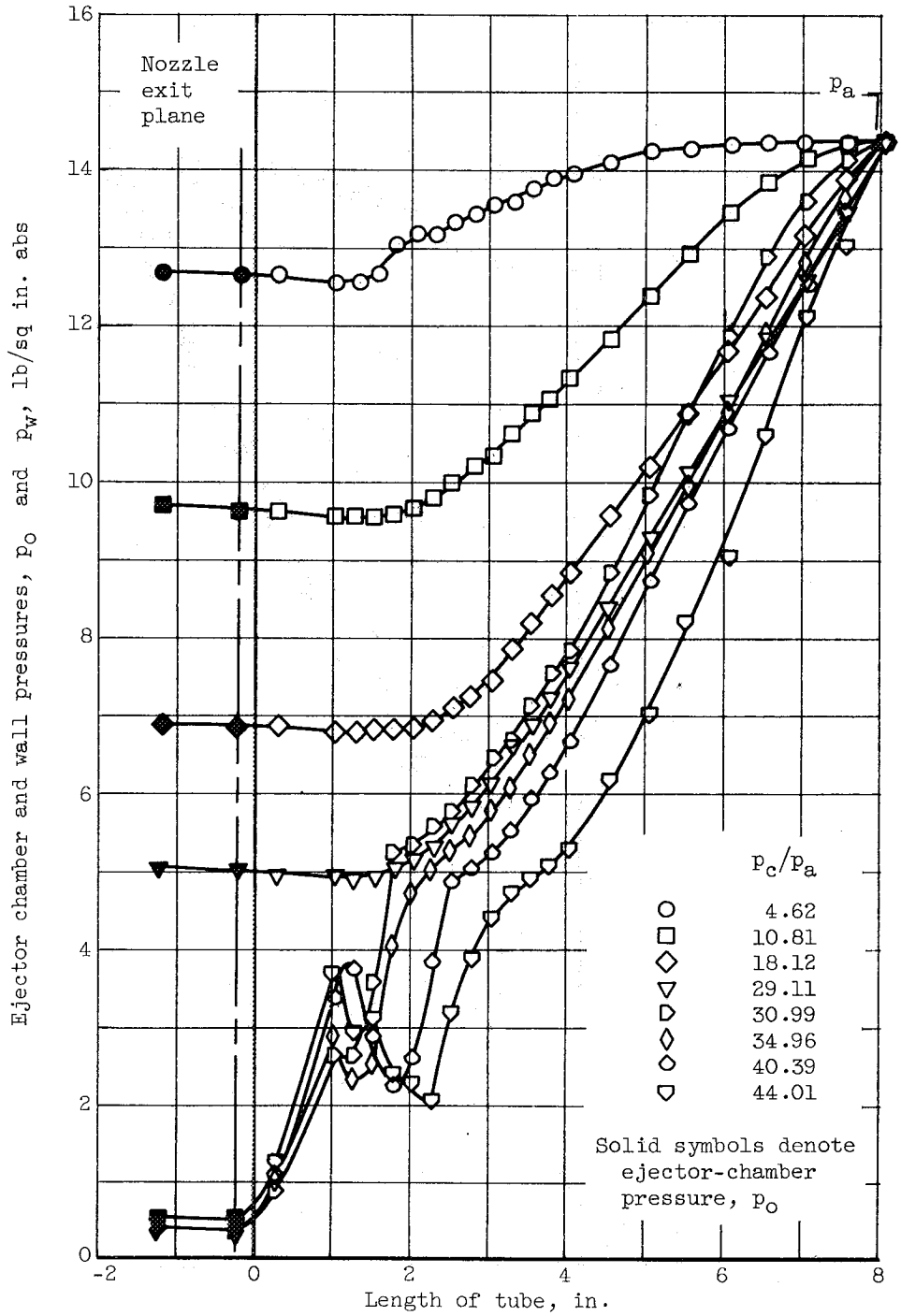


(c) L/D, 5.33; D, 1.5 inches.

Figure 8. - Continued. Ejector chamber and wall pressure distributions for constant-diameter ejector tubes having various L/D. Ejector-tube area ratio, $A_3/A_t$, 36; primary-nozzle area ratio, 9; no secondary flow.

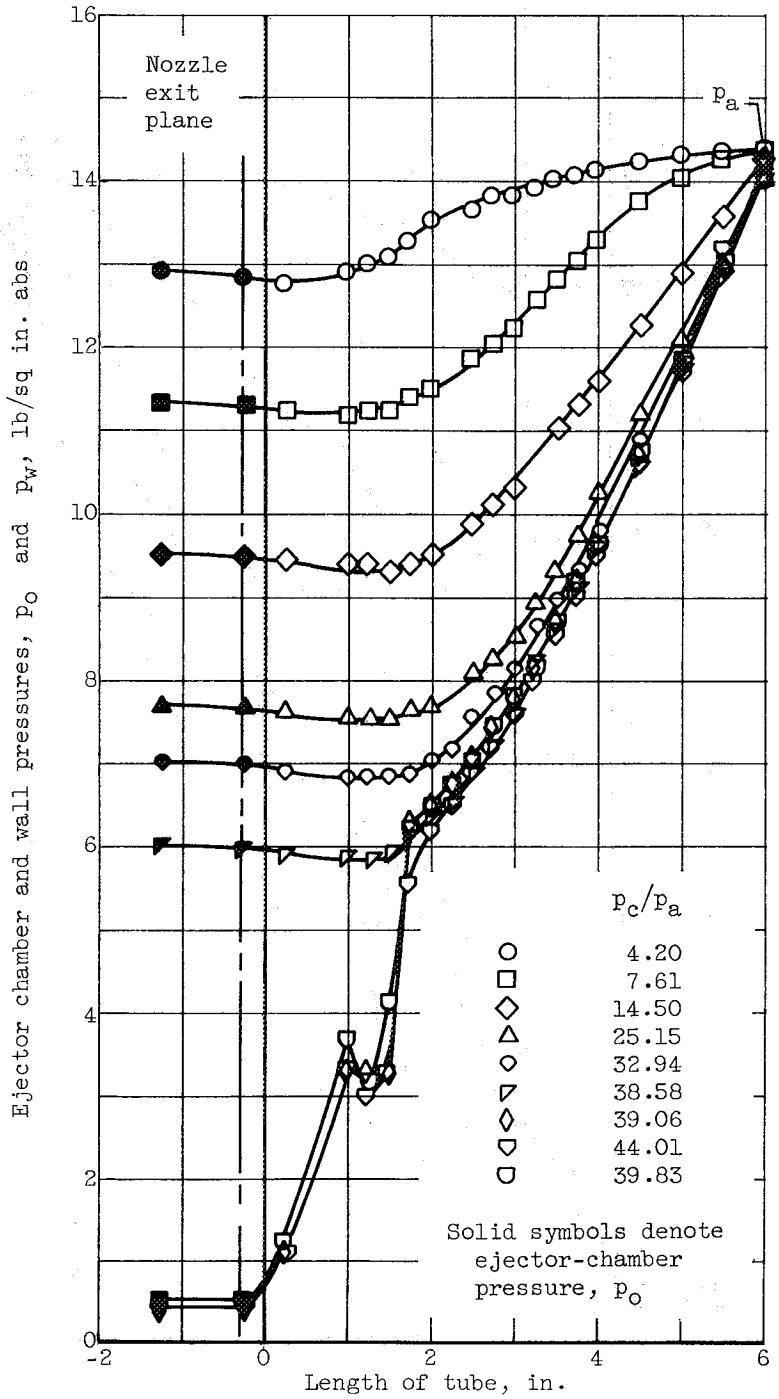


(d) L/D, 4.00; D, 1.5 inches.

Figure 8. - Continued. Ejector chamber and wall pressure distributions for constant-diameter ejector tubes having various L/D. Ejector-tube area ratio, $A_3/A_t$, 36; primary-nozzle area ratio, 9; no secondary flow.

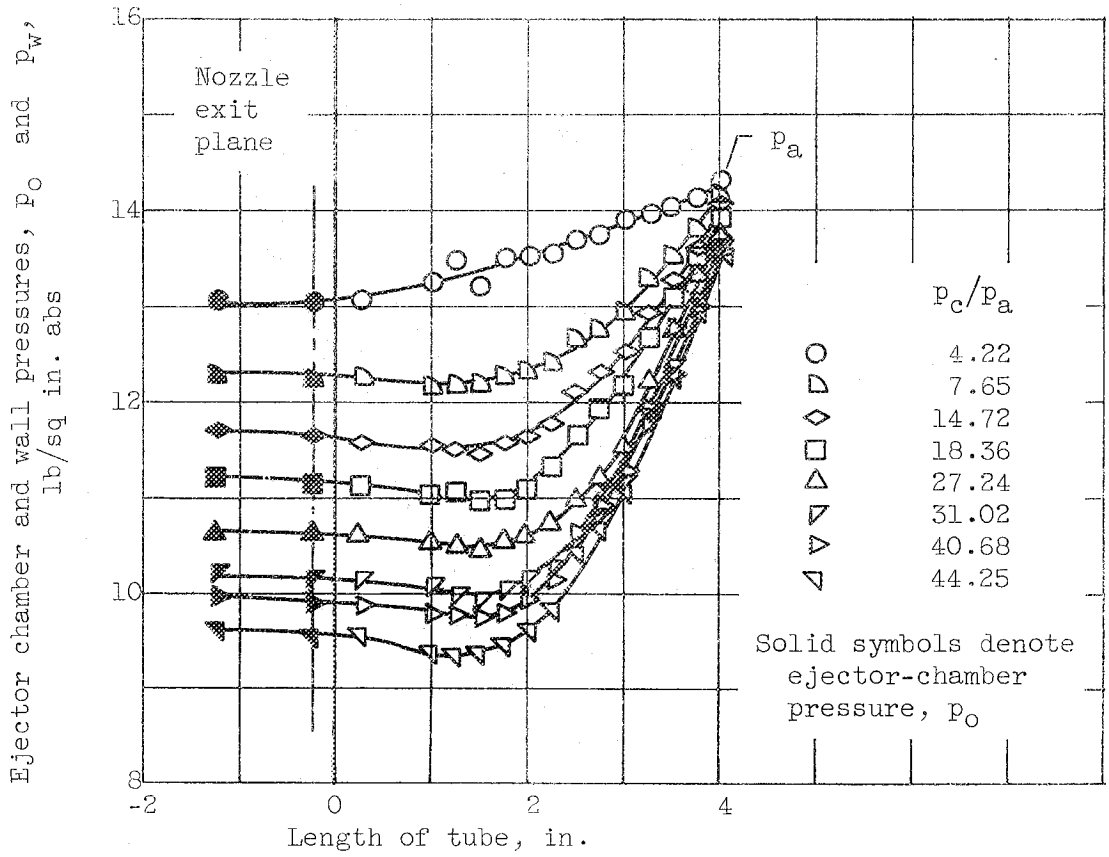


(e) L/D, 2.67; D, 1.5 inches.

Figure 8. - Concluded. Ejector chamber and wall pressure distributions for constant-diameter ejector tubes having various L/D. Ejector-tube area ratio, $A_3/A_t$, 36; primary-nozzle area ratio, 9; no secondary flow.

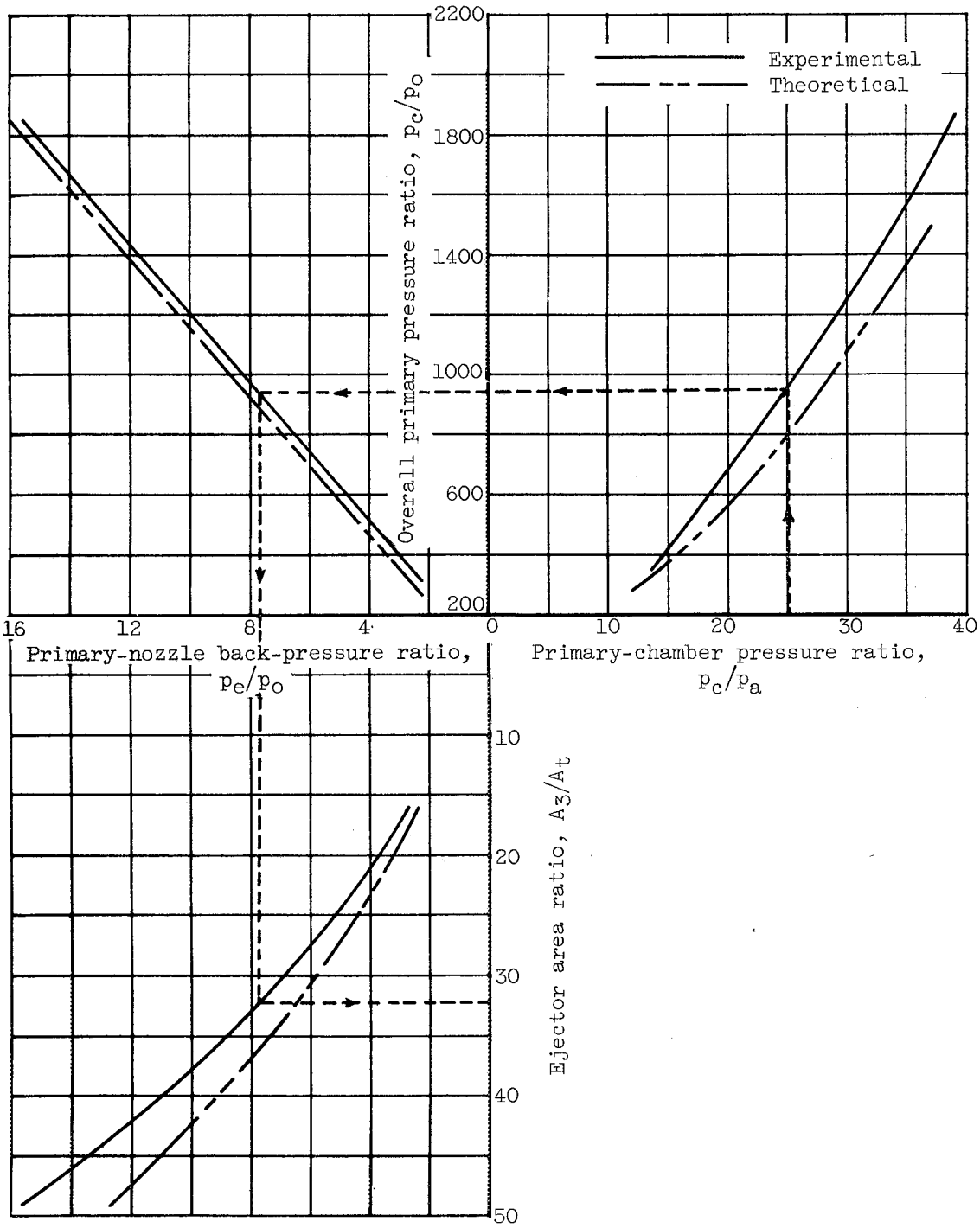


Figure 9. - Design parameters for obtaining minimum ejector chamber pressure ratio. Cylindrical ejector with sufficient tube length; primary-nozzle area ratio, 9; no secondary flow.